PERGAMON

International Journal of Heat and Mass Transfer 42 (1999) 4567–4578

International Journal of HEAT and MASS TRANSFER

www.elsevier.com/locate/ijhmt

Analysis of the absorption process on a horizontal tube using Navier–Stokes equations with surface-tension effects

J.K. Min, D.H. Choi*

Department of Mechanical Engineering, Korea Advanced Institute of Science and Technology, Taejon 305-701, South Korea

Received 18 September 1998; received in revised form 12 February 1999

Abstract

A Navier–Stokes procedure has been developed to investigate the absorption phenomena about the free-falling film flow on a horizontal tube. The fully elliptic equations of momentum, temperature and concentration are solved by using the SIMPLER algorithm, which incorporates the QUICK scheme and the incomplete Cholesky conjugate gradient method for accuracy and efficiency. Taking account of the surface-tension effects, the free-surface location is carefully traced by the MAC method in a time-accurate manner. The details of the flow and heat/mass transfer phenomena, such as the free-surface location, the streamlines, the formation of recirculating region and the rate of absorption, are seen to be well captured. The results are presented for various flow rates; the surface tension is found to play an important role in dictating the flow field especially when the flow rate is low. © 1999 Elsevier Science Ltd. All rights reserved.

1. Introduction

Growing demand for the environmentally viable alternate energy sources has renewed interest in the absorption refrigeration system in recent years. One of the most vital parts of the system is the absorber as it often dictates the system performance. The absorption process is very complex to analyze since it involves not only the heat and mass transfer associated with the absorption but also the film flow in which the free surface is determined as part of the solution. A typical absorber is composed of an array of horizontal cooling tubes; the absorbent solution absorbs the low pressure refrigerant vapor while flowing down along the tube surface.

On an isolated single tube (see Fig. 1), most of the earlier attempts to tackle this problem considered only the heat/mass transfer aspect of the process by relying on the assumed or simplified velocity profiles [1,2]. For the film flow on the horizontal tube, Choudhury et al. [3] assumed that the flow is fully developed and used Nusselt's analytic velocity profile and thickness [4] to predict the heat/mass transfer process. Andberg and Vliet [5] made use of the momentum equation to compute the thickness from the continuity of the flow. However, the equations adopted so far have been of the boundary-layer type to achieve computational efficiency. The main difficulty of this approach arises in the vicinity of the upper and lower stagnation points where the thin boundary-layer approximation breaks down and the surface tension becomes substantial due to the abrupt change in the film-surface curvature. Also the procedure is not suitable for flows that exhibit the wavy free surface, which is commonly observed in

* Corresponding author. Tel.: +82-42-869-3018; fax: +82-42-869-3210.

E-mail address: dhchoi@hanbit.kaist.ac.kr (D.H. Choi)

0017-9310/99/$ - see front matter
PII: S0017-9310(99)00104-0

Nomenclature

Ar	Archimedes number, Eq. (18)
C	concentration
c_p	specific heat
D	diffusion coefficient
e_{ij}	rate of strain tensor
Fr	Froud number, Eq. (5)
g	gravity
$\overline{Ha}$	heat of absorption
h_M	mass-transfer coefficient
h_T	heat-transfer coefficient
Ja	Jacob number, Eq. (14)
k	thermal conductivity
Le	Lewis number, Eq. (14)
m''	mass flux
$\mathbf{n}$, n_i	unit normal vector
Nu	Nusselt number, Eq. (19)
p	pressure
Pr	Prandtl number, Eq. (5)
q''	heat flux
R	tube radius
Re	Reynolds number, Eqs. (5) and (18)
Sc	Schmidt number, Eq. (5)
Sh	Sherwood number, Eq. (19)
T	temperature
t	time
$\mathbf{t}$, t_i	unit tangential vector
$\mathbf{u}$, u_i	velocity vector
v_0	inlet velocity
We	Weber number, Eq. (11)
$\mathbf{x}$	position vector

Greek symbols

α	thermal diffusivity
Γ	mass flow rate
δ	film thickness
θ	angle measured from the upper stagnation point
κ	curvature of the free surface
μ	viscosity
ν	kinematic viscosity
ξ, η	transformed coordinates
ρ	density
σ	surface-tension coefficient

Subscripts

0	inlet
e	equilibrium
f	film
s	free surface
v	vapor
w	wall

Superscripts

*	dimensionless variables

a wide range of Reynolds numbers [6]. To overcome these difficulties, one may resort to a procedure based on the Navier–Stokes equations with an accurate free-surface tracking method.

The purpose of this paper is to develop a such procedure that accounts for the surface-tension effects to examine the details of the absorption process especially near the stagnation points on a horizontal tube. To authors' knowledge, little has been reported in this regard and how big a change this would make is largely unanswered; a successful procedure may have broader application in similar situations, such as heat exchangers that accompany the condensation and evaporation.

2. Solution procedure

We consider single isolated tube on which the film flow is initiated by the absorbent solution falling from the upper row as shown in Fig. 1. For constant fluid properties, the continuity, momentum, energy and diffusion equations for two-dimensional incompressible unsteady laminar film flows are written as:

$$\nabla^* \cdot \mathbf{u}^* = 0 \tag{1}$$

$$\frac{\partial \mathbf{u}^*}{\partial t^*} + (\mathbf{u}^* \cdot \nabla^*)\mathbf{u}^* = -\nabla^* p^* + \frac{1}{Re}\nabla^{*2}\mathbf{u}^* - \frac{1}{Fr}\mathbf{j} \tag{2}$$

$$\frac{\partial T^*}{\partial t^*} + (\mathbf{u}^* \cdot \nabla^*)T^* = \frac{1}{RePr}\nabla^{*2}T^* \tag{3}$$

$$\frac{\partial C^*}{\partial t^*} + (\mathbf{u}^* \cdot \nabla^*)C^* = \frac{1}{ReSc}\nabla^{*2}C^* \tag{4}$$

where the dimensionless variables denoted by the superscript * are defined as

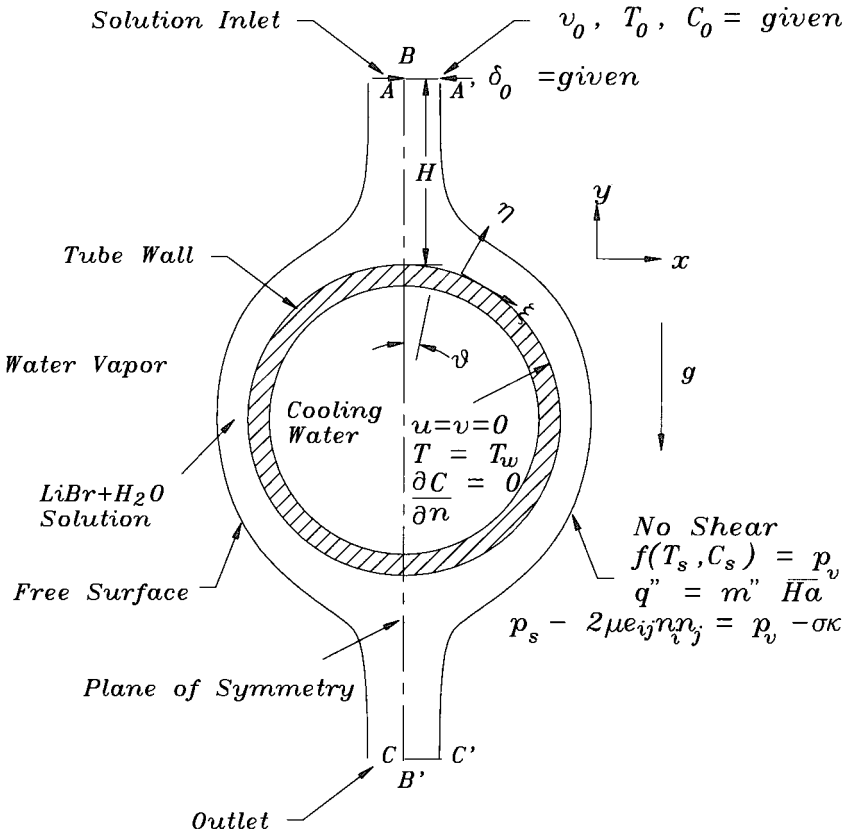

Fig. 1. Schematic of the film flow and boundary conditions.

$$\mathbf{x}^* = \frac{\mathbf{x}}{\delta_0}, \quad t^* = \frac{t}{\delta_0/v_0}$$

$$\mathbf{u} = \frac{\mathbf{u}}{v_0}, \quad p^* = \frac{p - p_v}{\rho v_0^2}, \quad T^* = \frac{T - T_w}{T_0 - T_w}, \quad C^* = \frac{C - C_{we}}{C_0 - C_{we}} \tag{5}$$

$$Re = \frac{\rho v_0 \delta_0}{\mu}, \quad Fr = \frac{v_0^2}{g\delta_0}, \quad Pr = \frac{\nu}{\alpha}, \quad Sc = \frac{\nu}{D}$$

and δ_0 = inlet film thickness; v_0 = inlet falling velocity; p_v = vapor pressure; T_0, T_w = inlet and wall temperatures, respectively; C_0, C_{we} = inlet concentration and equilibrium concentration of solution at T_w and p_v, respectively. Here $\mathbf{u}$ is the velocity vector, p the pressure, T the temperature and C the concentration. The Lagrangian equation of motion for the marker particles distributed on the free surface is also solved to update the new free-surface location:

$$\frac{d\mathbf{x}_s^*}{dt^*} = \mathbf{u}_s^* \tag{6}$$

The associated boundary conditions for the system are

• solid wall:

$$\mathbf{u}^* = 0, \quad T^* = 0, \quad \frac{\partial C^*}{\partial n^*} = 0$$

• inlet (AA′):

$$\mathbf{u}^* = \mathbf{u}_0^*, \quad T^* = C^* = 1$$

• plane of symmetry (BB′):

$$u_n^* = 0, \quad \frac{\partial u_t^*}{\partial n^*} = \frac{\partial T^*}{\partial n^*} = \frac{\partial C^*}{\partial n^*} = 0 \tag{7}$$

• outlet (CC′): negligible diffusion in streamwise direction [7].

The magnitude of inlet velocity v_0 is assumed to be the free-fall speed from the upper tube, i.e. $v_0 = \sqrt{2gd}$

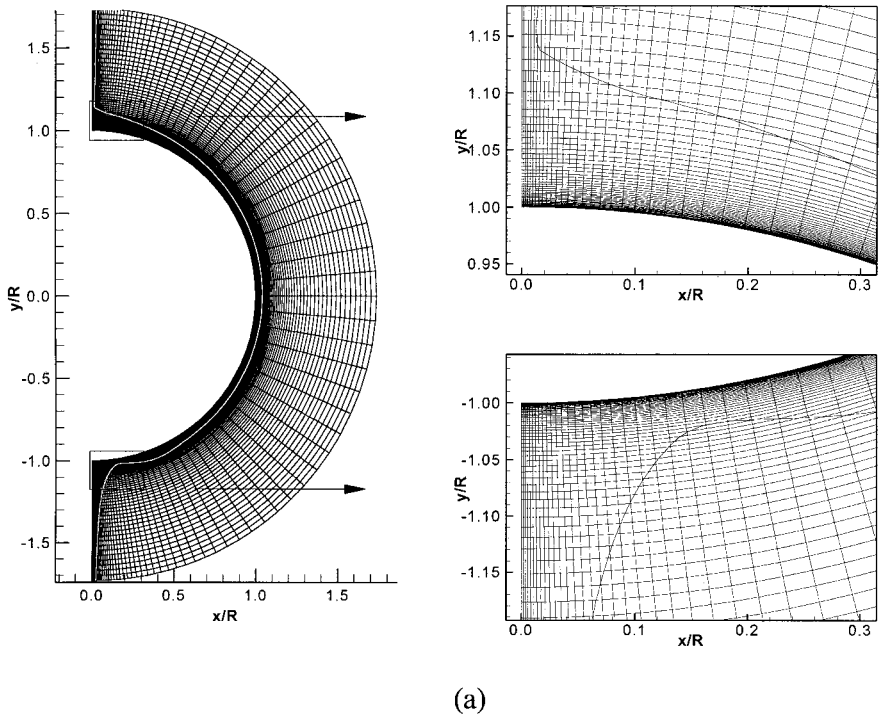

(a)

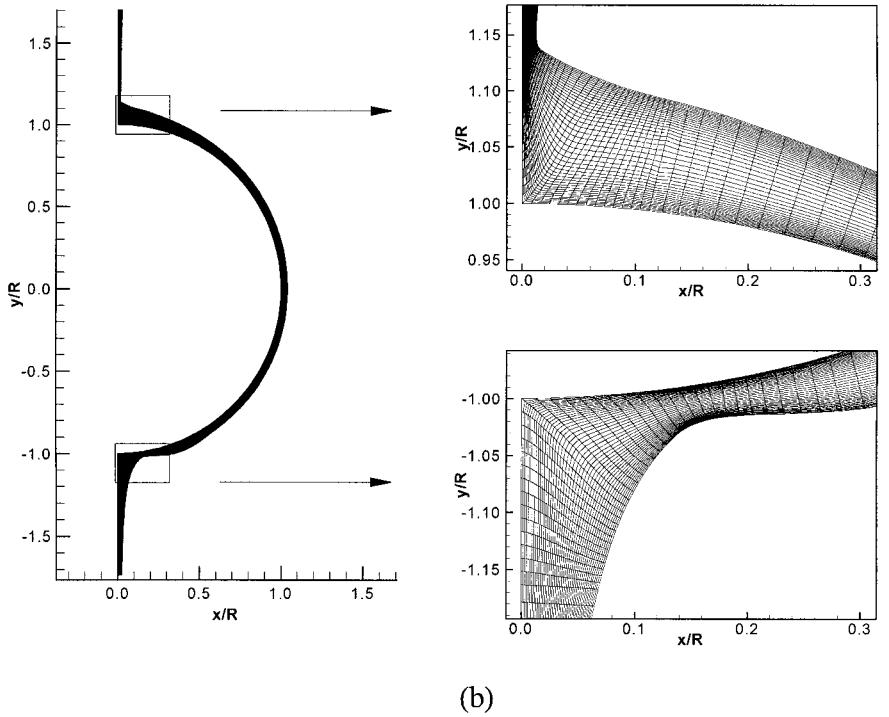

(b)

Fig. 2. Typical grid configurations for $Re = 16.7$: (a) 101×71 orthogonal grid for unsteady MAC calculation, (b) 198×45 non-orthogonal grid for steady calculations.

where d is the distance between the lower stagnation point of the upper tube and the inlet plane; the inlet film thickness δ_0 is then determined from the specified flow rate Γ:

$$\Gamma = \rho v_0 \delta_0. \tag{8}$$

The parabolic outlet condition is due to Stuhlträger et al. [7]; a linear extrapolation is used to follow the particle trajectory and to get outflow boundary values. At the free surface, the shear stress is negligibly small and thus the velocity field must satisfy

$$e^*_{ij} n^*_i t^*_j = 0 \tag{9}$$

along with the continuity at the surface cell. Here e^*_{ij} is the rate of strain tensor and n_j, t_j are the normal and tangential vector components in j-direction. The dynamic condition at the surface, which includes the surface-tension effects, may be expressed as

$$p^*_s = \frac{2}{Re} e^*_{ij} n^*_i n^*_j - \frac{1}{We}\kappa^* \tag{10}$$

where the Weber number is defined by

$$We = \frac{\rho v_0^2 \delta_0}{\sigma} = \frac{\Gamma v_0}{\sigma} \tag{11}$$

and the σ and κ are the surface-tension coefficient and curvature of the free surface, respectively. The boundary conditions for the temperature and concentration at the free surface are expressed by using Fick's law and the vapor-pressure-equilibrium condition:

$$\left.\frac{\partial T^*}{\partial n^*}\right|_s = -\frac{Le}{Ja}\frac{1}{C_s}\left.\frac{\partial C^*}{\partial n^*}\right|_s \tag{12}$$

$$C^*_s = EqT^*_s \tag{13}$$

where

$$Le = \frac{D}{\alpha}, \quad Ja = \frac{c_p(T_0 - T_w)}{\overline{Ha}(C_0 - C_{we})}, \quad Eq = \frac{A_1(T_0 - T_w)}{(C_0 - C_{we})} \tag{14}$$

and the linear absorbent assumption for a fixed pressure is

$$C_s = A_1 T_s + A_2. \tag{15}$$

The new dimensionless number Eq is the measure of the initial deviation from the equilibrium state: it is 1 when in equilibrium and less than 1 otherwise.

Observing that the continuity and momentum equations can be decoupled from the system since the free-convection effects and the rate of mass transfer due to absorption are negligibly small, we break the solution procedure into two: the continuity and momentum equations are solved first for the velocity field and the free-surface location; the energy and concentration equations are then solved only in the film flow region over which a new nonorthogonal grid is fitted. The velocity field is also recalculated on a new grid in the latter part of the solution to avoid any interpolation error. In other words, the orthogonal grid is used only to obtain the free-surface location, which is treated as a fixed boundary in the following calculation. This two-grid, two-step approach is advantageous because an orthogonal grid is more convenient in determining the free-surface location which moves around before convergence while a nonorthogonal general grid is better suited when dealing with an arbitrarily shaped fixed computational domain as in the present heat/mass transfer analysis.

Using the staggered grid, the SIMPLER algorithm of Patankar [8] is adopted to solve the governing Eqs. (1)–(4); the MAC method proposed by Tanaka and Takaki [9] is suitably modified and incorporated in the procedure to track the free-surface location. The steady state is considered to be achieved if the time-averaged velocity components, the film thickness, and the root-mean-square (r.m.s.) velocity converge, or all the initial marker particles have gone out the domain as suggested by Stuhlträger et al. [7].

3. Computational conditions and assumptions

The cases examined are the LiBr–H_2O solution flowing down on the tube surface for a range of Reynolds numbers, based on the inlet velocity and width, from 12.5 to 166.7. The tube radius, which is interrelated with the flow rate (or Re) in the analysis, is kept constant for all calculations. Note that, since we vary the Reynolds number, it suffices to consider just one tube size. The size may be given an arbitrary value for the present purpose, however, the value of 9.525 mm, which is taken from a commercially manufactured absorption-type refrigerator, is used in the study. The inlet of the computational domain is placed at 7 mm above the upper stagnation point (see Fig. 1) and the initial velocity v_0 comes out as 0.2237 m/s. The fully developed film thickness to the tube radius in the present Re range varies from 0.1 to 0.15.

It is proper to mention here that some fluctuating behavior is observed at lower Re range. Whether the phenomenon is real or numerical aberration is yet to be answered, however, as the unsteadiness is not significant, we assume the flow is steady and take the long-time average to determine the free-surface location. As described in the previous section, the free-surface location is first obtained by solving Eqs. (1)

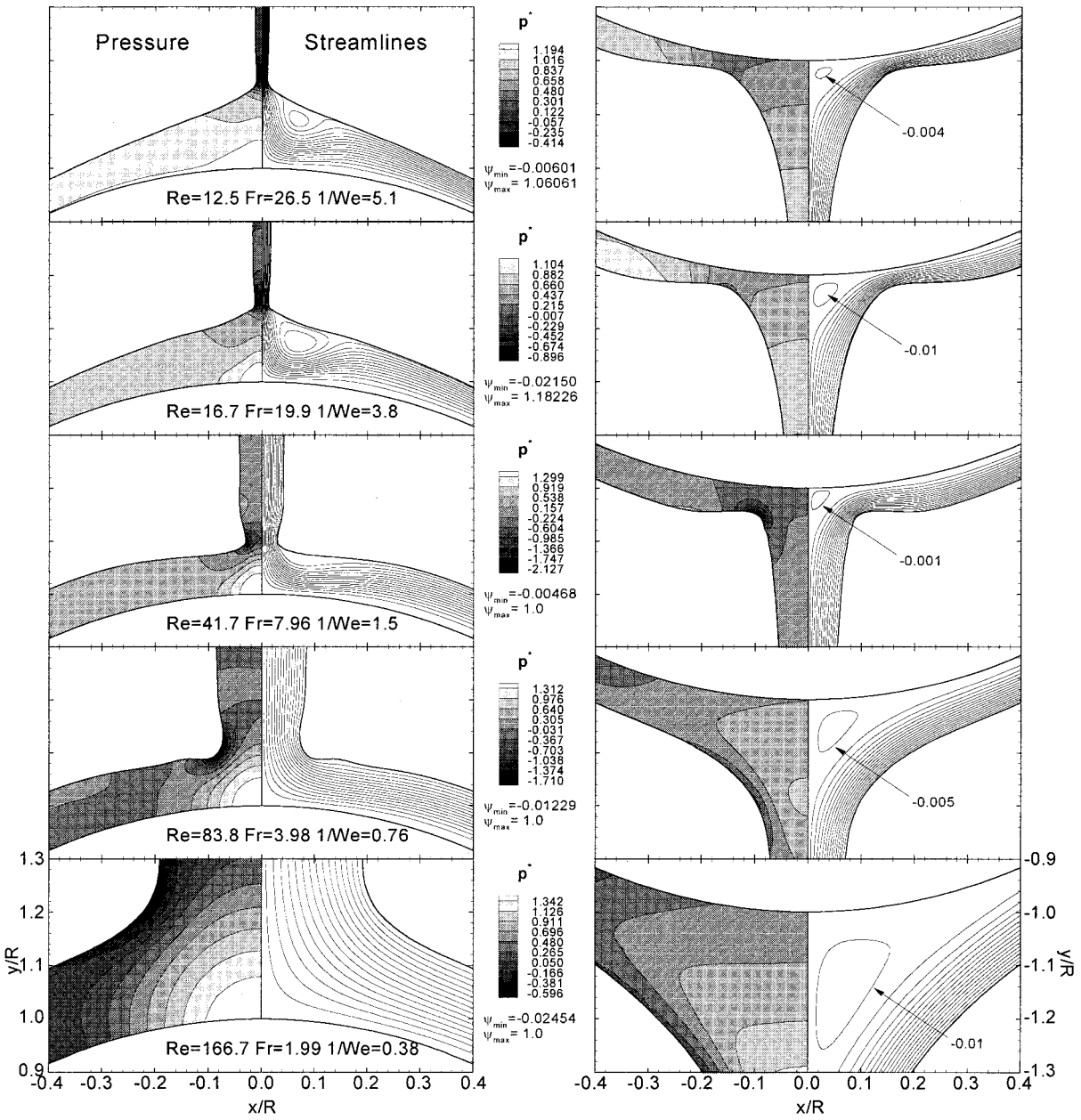

Fig. 3. Streamlines and pressure field for various flow rates.

and (2) with associated boundary conditions on a 101×71 non-uniform orthogonal grid in a time-marching manner. Upon reaching the steady state, a new grid (198×45), which is nonorthogonal but conforms to the fixed free surface, is generated for a more accurate steady-state heat and mass transfer analysis. The grid is chosen after a thorough numerical test and the details will be given later. The two grid systems along with the free-surface location are displayed in Fig. 2.

4. Results and discussions

The streamline patterns and pressure fields near the upper and lower stagnation points are shown in Fig. 3

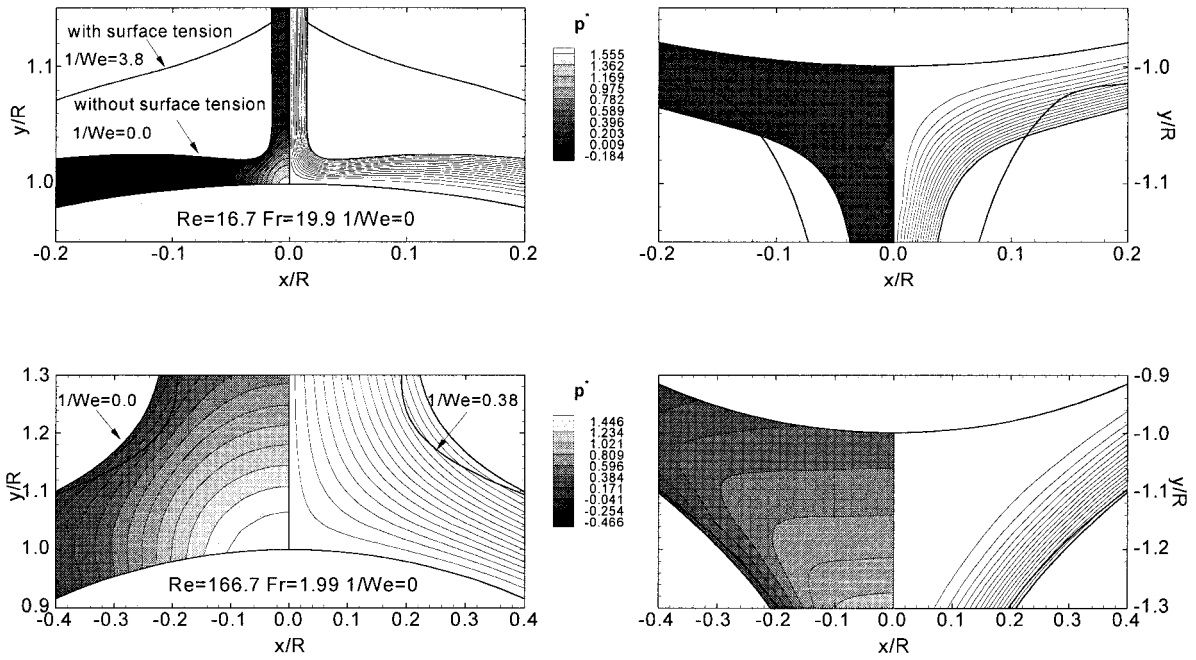

Fig. 4. Streamlines and pressure field without surface-tension effects for $Re = 16.7$ and 166.7.

for various flow rates. Contrary to the common belief that the film is thinner when the flow rate is smaller, the stagnation film thickness appears to increase as Re decreases when $Re < 40$. This, what seems to be an unusual phenomenon, may be explained as follows: the film, coming out of the stagnation point, becomes thinner as the flow accelerates. However, the friction acting on this thin film retards the flow and makes the film thickness increase. If the film thickness were to increase very much, it backflows and submerges the thin upstream region. For $Re = 12.5$ and 16.7, a sizable region of recirculation develops in the stagnation region. As the flow rate increases, the recirculating region disappears and the film thickens to accommodate the increased flow rate. The flow exhibits the similar behavior near the lower stagnation point: the strength of the recirculating region, which is present for all cases, is smallest when $Re \approx 41.7$ and the fluid stays on the tube longest at that Reynolds number.

To examine the effects of the surface tension, calculations have been repeated for $Re = 16.7$ and 166.7 without the surface-tension effects, i.e. $1/We = 0$ for both cases. The results are compared with those with the surface-tension effects in Fig. 4. Two results are quite distinct in the low Re regime while they are closely matched for the high Re flow. For $Re = 16.7$, the calculation without the surface-tension effects is unable to predict the recirculating region in the upper stagnation region and gives a very thin film flow. The results resemble the boundary-layer-type calculation by Andberg and Vliet [5]. When the flow rate is large, the surface-tension force diminishes and two calculations give nearly identical results. The boundary-layer-type calculation is expected to be effective in this flow regime.

The calculated film shape in the entire domain is plotted in Fig. 5. Compared in the figure are the Nusselt solution

$$\frac{\delta}{2R} = 0.909 Re_f^{1/3} Ar^{-1/3} (\sin\ \theta)^{-1/3} \tag{16}$$

and the empirical correlation by Rogers and Goindi [10]

$$\frac{\delta}{2R} = 3.716 Re_f^{0.174} Ar^{-1/3} (\sin\ \theta)^{-1/3} \tag{17}$$

where the film Reynolds number and Archimedes number are defined by

$$Re_f = \frac{4\Gamma}{\mu}, \quad Ar = \frac{8g\rho^2 R^3}{\mu^2}. \tag{18}$$

In light of the reasons stated above, it is not surprising to see the agreement among the results is poor in the stagnation region. The agreement is mixed however, in the tube side: While the calculated film thickness follows closely the Nusselt solution when the flow rate is low, the gap between the two becomes large as the flow rate increases since it takes longer to attain the

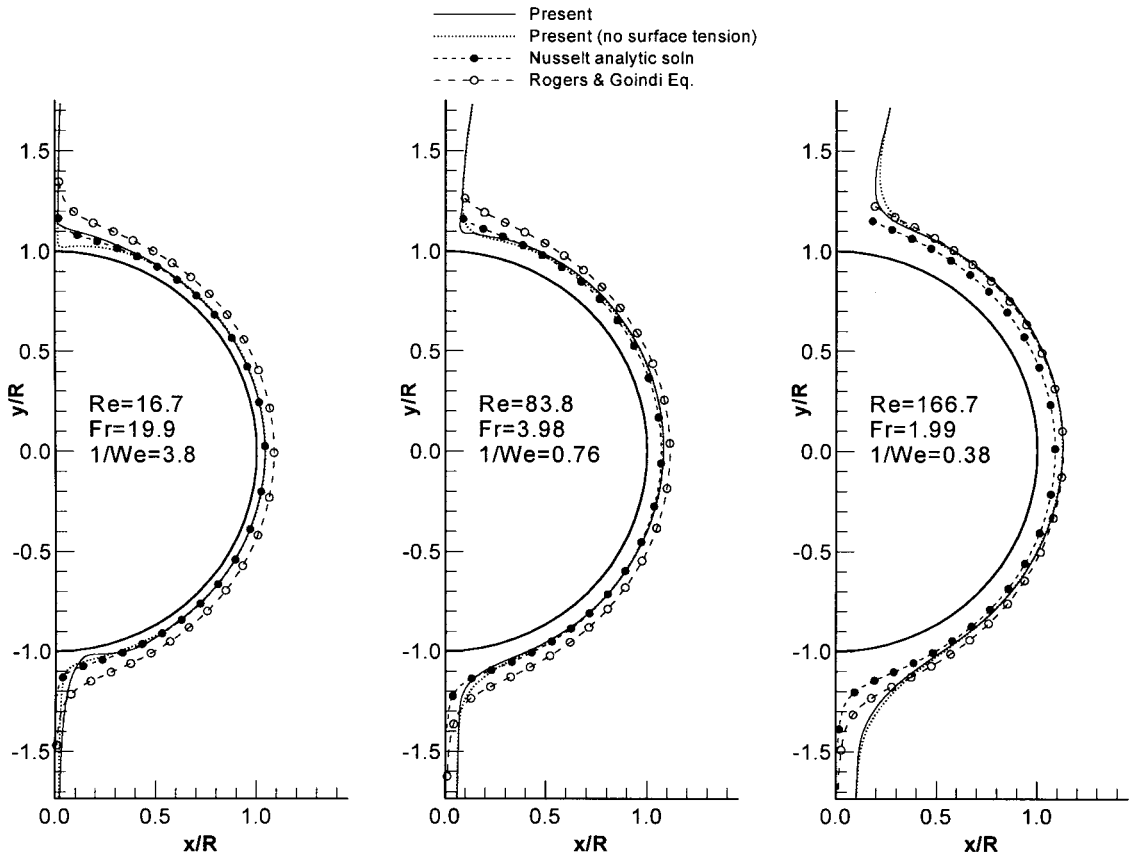

Fig. 5. Free-surface shapes for various flow rates.

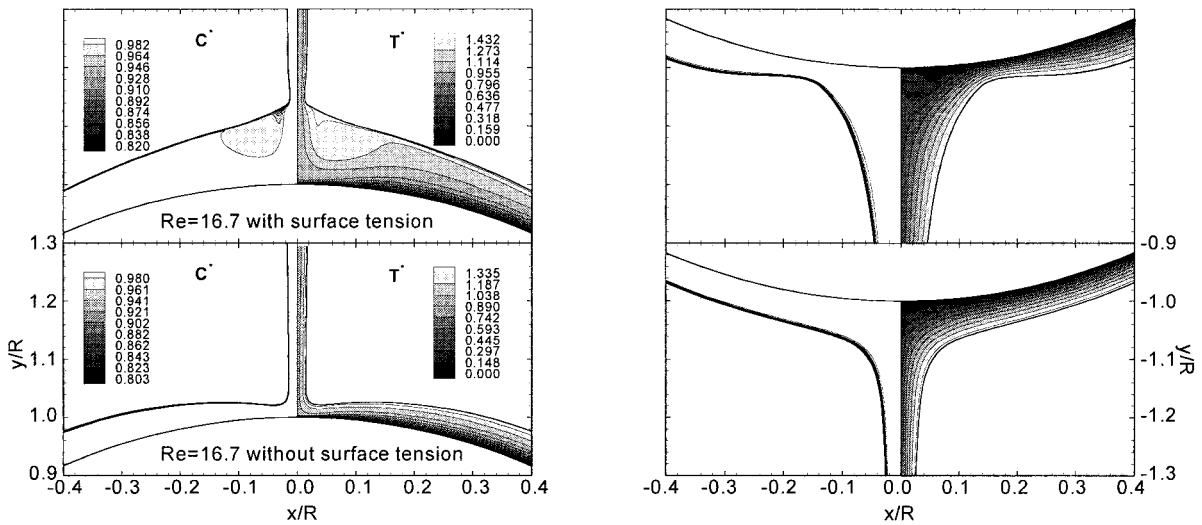

Fig. 6. Temperature and concentration distributions with/without surface-tension effects.

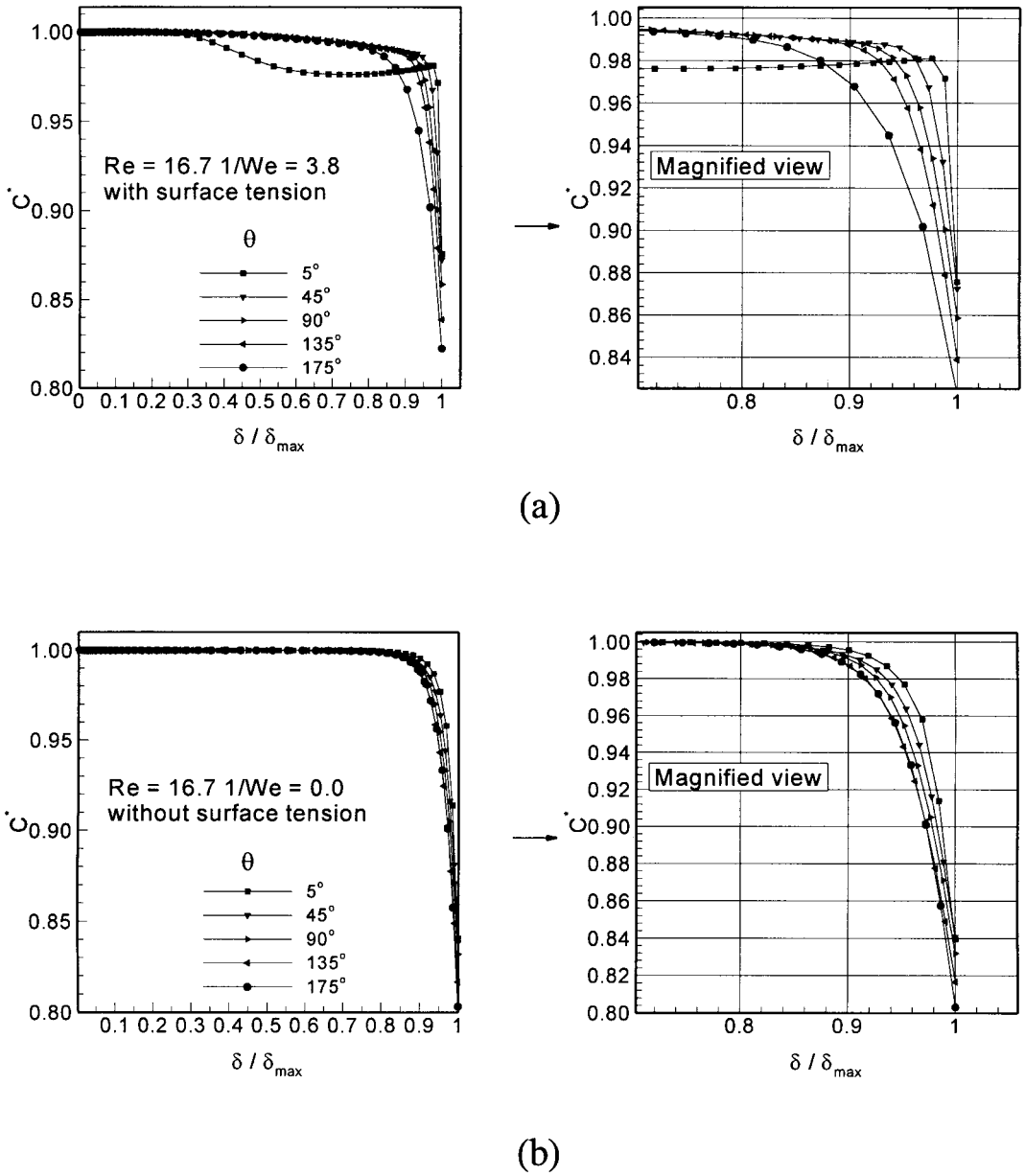

Fig. 7. Concentration profiles for various streamwise sections for $Re = 16.7$: (a) with surface-tension effects, (b) without surface-tension effects.

fully developed state. The correlation by Rogers and Goindi, on the other hand, looks good when $Re = 166.7$ but becomes poor for the other two smaller Reynolds-number cases. The experiments by Rogers and Goindi was done in the film Reynolds number ranging $400 < Re_f < 2000$, which is much larger than that used in the present paper. One may conclude that this experimental relation cannot be extrapolated to the small Reynolds numbers for which the surface-tension effects are important.

We now turn our attention to the heat and mass transfer aspect of the problem. Among various flow rates, the results for $Re = 16.7$, which lies in the typical operating range, is presented. The wall temperature is maintained at 30°C while the temperature and the concentration at the inlet are given by 40°C and 0.612,

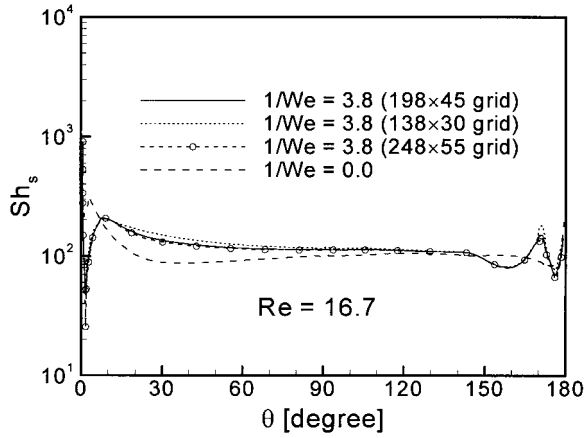

Fig. 8. Distribution of absorption rate at the free surface for $Re = 16.7$.

respectively. The concentration of 0.612 is the equilibrium concentration at 48°C and 1 kPa, which is the vapor pressure in the absorber. It is noted that, since the inlet temperature is lower than the equilibrium temperature for this concentration, the absorption occurs as soon as the LiBr–H_2O solution enters the domain. For conditions stated above, the nondimensional parameters take the following values: $Pr = 21.4$, $Sc = 2456$, $Le = 0.008$, $Eq = 0.573$ and $Ja = 0.058$.

The concentration and temperature fields near the upper and lower stagnation points are shown in Fig. 6. The regions of recirculation seen in Fig. 3 are readily identifiable in the figure: the one near the upper stagnation point is characterized by the high temperature and the low concentration. The tiny recirculation region near the lower stagnation point appears to have little influence on the concentration field. The temperature in the region, however, is lower as the fluid is trapped near the cooler wall. Note that, due to the relatively large Schmidt number, the concentration varies mostly in a thin region adjacent to the free surface. Needless to say sufficiently many grids are needed to accurately resolve this region. Fig. 7 depicts the concentration distribution across the layer at various streamwise sections. The abscissa denotes the distance from the tube wall normalized by the local film thickness, δ_{max}. The rapid variation of the concentration near the free surface appears to be well captured at all sections. We will come back to this point later in Fig. 8. Among the profiles, the one at $\theta = 5°$ with surface tension (Fig. 7(a)) may be singled out for its odd behavior. The dip in the profile in the middle of the layer is due to the flow recirculation described earlier. The backflow of the weak solution in the outer part of the layer is responsible for this phenomenon as it mixes with the strong solution inside.

The films, regardless the surface-tension effects, eventually reach the same fully developed thickness. As the layer thins, the temperature gradient normal to the free surface increases and so does the rate of absorption. The thickening of the film does the opposite. This phenomenon is well illustrated in Fig. 8, which compares the Sherwood number

$$Sh_s = \frac{h_{Ms}R}{D} = \frac{m_s'' R}{\rho(C_0 - C_{we})D} \tag{19}$$

along the free surface, where m_s'' denotes the rate of absorption at the free surface. For the case with the surface-tension effects, the absorption rate drops off sharply in the early stage due to the thick layer but recovers handsomely as the layer begins to thin down. As a further proof that the present grid (198 × 45) is adequate, the results obtained with two other grids (138 × 30, 248 × 55) are also compared in the figure. It shows that the results of the two finer grids are nearly identical and confirms the solution is accurate. The absorption in the other case (without surface-tension effects) decreases continuously until it levels off for $\theta > 30°$. The discrepancy between the two, which persists even after the film thickness coincide, say $\theta > 30°$, may be attributed to the inertia or transient effects. The higher rate of absorption generates more heat and sends the temperature higher. This in turn increases the normal temperature gradient and also the rate of absorption. In other words, the cycle is self-sustained and goes on until the concentration and temperature fields fully develop. This argument is supported by the Nusselt number distribution along the tube wall shown in Fig. 9. The Nusselt number is defined as

$$Nu_w = \frac{h_{Tw}R}{k} = \frac{q_w'' R}{(T_0 - T_w)k} \tag{20}$$

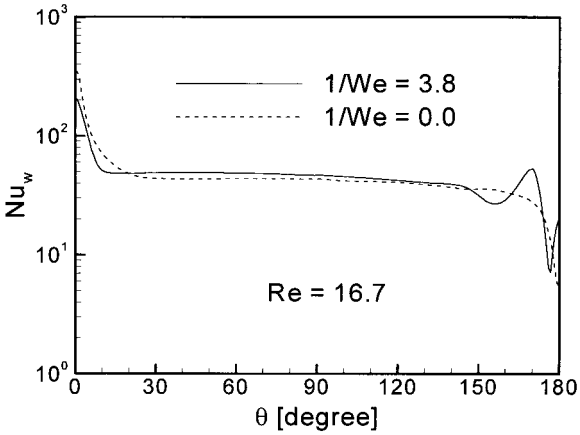

Fig. 9. Heat flux at the tube wall for $Re = 16.7$.

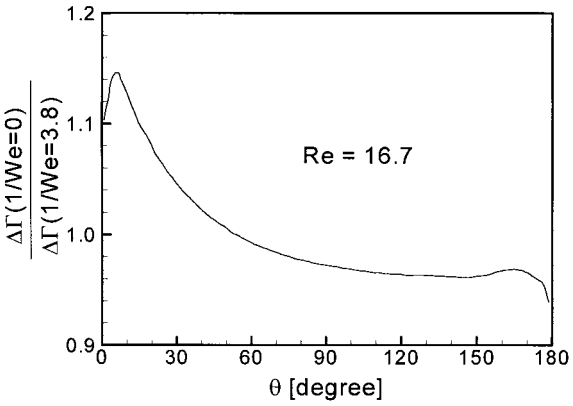

Fig. 10. Ratio of cumulative absorption (surface-tension-free to with-surface-tension cases) along the film surface for $Re = 16.7$.

where q''_w denotes the heat flux through the tube wall. The lower heat flux in the region of recirculation compared to the attached-flow case is due to the thicker layer and is consistent with the fact observed in Fig. 8. However, comparing with Fig. 8, there is a time lag between the heat generation by absorption and the heat removal through the wall. This suggests that the increased absorption leads to the increased heat flux and not the other way around.

The rapid variation in Sh_s and Nu_w near the lower stagnation point can be explained by the film shape in that region. Comparing with the surface-tension-free case, the film goes through thicker ($\theta \approx 150^\circ$), thinner ($\theta \approx 170^\circ$), and then thicker again pattern to produce the wiggly behavior in these quantities. The cumulative absorption relative to that with the surface-tension effects is plotted in Fig. 10. As has been witnessed, the cumulative absorption for the surface-tension-free case is larger until it is overtaken by the other at about $\theta = 50^\circ$. The total absorption with the surface-tension effects comes out approximately 4% larger than that without.

So far, we have examined one inlet-condition case and demonstrated that the flow and heat/mass transfer characteristics are quite distinct when the surface-tension effects are included. We believe that the change in the initial and/or boundary conditions leads to a variety of situations and a parametric study would be very helpful in predicting the absorber performance.

5. Conclusions

The absorption process about the free-falling LiBr–H_2O film flow on a horizontal tube has been investigated. This novel approach, that solves the fully elliptic governing equations and takes account of the surface-tension effects, allows one to capture details of the flow field which are quite distinct from those obtained by a boundary-layer-type procedure. It has been shown that a small but hydrodynamically significant region of recirculation forms next to the free surface near the stagnation point and, consequently, alters the mass transfer characteristics as well as the absorption rate. The phenomenon becomes more pronounced as the flow rate decreases.

It is clearly demonstrated that the use of the Navier–Stokes equations with full consideration of the surface-tension effects is essential to accurately predict the absorber performance. A thorough parametric study regarding the initial and boundary conditions on temperature and concentration would yield more useful information on the range where this procedure is most needed.

Acknowledgement

This work was supported by the Korea Science and Engineering Foundation under Grant 971-1008-053-1. The support is gratefully acknowledged.

References

[1] N.I. Grigor'eva, V.E. Nakoryakov, Exact solution of combined heat- and mass-transfer problem during film absorption, Journal of Engineering Physics 33 (1977) 1349–1353.

[2] G. Grossman, Simultaneous heat and mass transfer in film absorbtion under laminar flow, Int. J. Heat Mass Transfer 26 (1983) 357–371.

[3] S.K. Choudhury, D. Hisajima, T. Ohuchi, A. Nishiguchi, T. Fukushima, S. Sakaguchi, Absorption of vapors into liquid films flowing over cooled horizontal tubes, ASHRAE Transactions: Research 99 (1993) 81–89.

[4] W. Nusselt, Die Oberflächenkondensation des Wasserdampfes, Z. Ver. dt. Ing. 60 (1916) 541–546.

[5] Andberg JW, Vliet GC Absorption of vapors into liquid films flowing over cooled horizontal tubes. In: Proceedings of the ASME/JSME Joint Thermal Engineering Conference, Honolulu, HI, 1987, pp. 533–541.

[6] H. Sabir, K.O. Suen, G.A. Vinnicombe, Investigation of effects of wave motion on the performance of a falling film absorber, Int. J. Heat Mass Transfer 39 (1996) 2463–2472.

[7] E. Stuhlträger, Y. Naridomi, A. Miyara, H. Uehara, Flow dynamics and heat transfer of a condensate film

on a vertical wall—I. Numerical analysis and flow dynamics, Int. J. Heat Mass Transfer 36 (1993) 1677–1686.

[8] S.V. Patankar, Numerical Heat Transfer and Fluid Flow, McGraw-Hill, New York, 1980, Chap. 6.

[9] A. Tanaka, R. Takaki, Analysis of pipe flow with free-surface Part I: numerical computation, Fluid Dynamics Research 13 (1994) 229–247.

[10] J.T. Rogers, S.S. Goindi, Experimental laminar falling film heat transfer coefficients on a large diameter horizontal tube, The Canadian Journal of Chemical Engineering 67 (1989) 560–568.